



## Supplementary Materials for

### **Glutamate triggers long-distance, calcium-based plant defense signaling**

Masatsugu Toyota\*, Dirk Spencer, Satoe Sawai-Toyota, Jiaqi Wang, Tong Zhang,  
Abraham J. Koo, Gregg A. Howe, Simon Gilroy\*

\*Corresponding author. Email: [mtoyota@mail.saitama-u.ac.jp](mailto:mtoyota@mail.saitama-u.ac.jp) (M.T.); [sgilroy@wisc.edu](mailto:sgilroy@wisc.edu) (S.G.)

Published 14 September 2018, *Science* **361**, 1112 (2018)  
DOI: 10.1126/science.aat7744

#### **This PDF file includes:**

Materials and Methods  
Figs. S1 to S16  
Tables S1 and S2  
Captions for Movies S1 to S13  
References

**Other Supplementary Materials for this manuscript include the following:**  
(available at [www.sciencemag.org/content/vol361/6407/1112/suppl/DC1](http://www.sciencemag.org/content/vol361/6407/1112/suppl/DC1))

Movies S1 to S13

## Materials and Methods

### Plant material and growth condition

Surface-sterilized seeds of *Arabidopsis thaliana* (Col-0) were sown on agar plates [1× MS salts, 1% (w/v) sucrose, 0.01% (w/v) myoinositol, 0.05% (w/v) MES and 0.5% (w/v) gellan gum; pH 5.8 adjusted with KOH] (23). After incubation in the dark at 4°C for 2d, plates were cultivated at 22°C in a growth chamber under continuous light (90–100 μmol m<sup>-2</sup> s<sup>-1</sup>) for 2–3 weeks prior to use. *glr3.3-1* (salk\_040458) and *glr3.3-2* (salk\_066009), *glr3.6-1/3.6a* (salk\_091801) and *glr3.6-2/3.6b* (salk\_035353) were kind gifts from Edgar Spalding (Department of Botany, University of Wisconsin, Madison), *glr3.3bglr3.6a* double mutants (salk\_077608/salk\_091801) were from Edward Farmer (Department of Plant Molecular Biology, University of Lausanne) and the PDLP5 overexpression lines, Jung-Youn Lee (Department of Plant and Soil Sciences, University of Delaware).

### DNA cloning and transformation

For the *p35S::GCaMP3* Ca<sup>2+</sup> biosensor construct, the GCaMP3 fragment, gifted by Loren Looger (Addgene plasmid #22692), was PCR amplified between XbaI and BamHI sites and inserted into the equivalent sites of a pAN19 vector containing the CaMV35S promoter (*p35S*). The entire cassette of *p35S::GCaMP3 NOS* was isolated by NotI digestion and ligated into the NotI site of the plant binary vector, pBIN20. This construct was transformed to *glr3.3* and *glr3.6* single mutants, the *glr3.3bglr3.6a* double mutant and the PDLP5 overexpression lines described above.

For the *pSUC2::GCaMP3* Ca<sup>2+</sup> biosensor construct, the promoter region of SUC2 (2092 bp, At1g22710), between HindIII and XbaI sites, was amplified by PCR from Arabidopsis genomic DNA, digested, and ligated into the equivalent sites of the pAN19 vector. The entire cassette of *pSUC2::GCaMP3 NOS* was isolated by NotI digestion and cloned into the NotI site of the pBIN20 vector.

For the *p35S::CHIB-iGluSnFR* apoplastic Glu biosensor construct, the basic chitinase (CHIB, AT3G12500) signal peptide (63 bp) from Arabidopsis genomic DNA was amplified between XbaI and BamHI sites by PCR and inserted into the corresponding sites of the pAN19 vector; the iGluSnFR fragment, a gift from Loren Looger (Addgene plasmid #41732), was amplified between BamHI and SmaI sites and inserted into the equivalent sites of the pAN19 vector. The entire cassette of *p35S::CHIB-iGluSnFR RbcSt* was isolated by NotI digestion and cloned into the NotI site of the plant binary vector, pBIN42.

The promoter region of *GLR3.6* (2011 bp, At3g51480) was PCR amplified between SphI and XbaI sites from genomic Arabidopsis DNA and inserted into the equivalent sites of the pAN19 vector. *GLR3.6* was amplified between XbaI and SmaI sites and inserted into the corresponding sites of the pAN19 vector. EFGP (pEZT-NL), a gift from David Ehrhardt, was amplified between SmaI and SacI sites and inserted within the compatible sites of the pAN19 vector. The entire cassette of *pGLR3.6::GLR3.6-EGFP NOS* was isolated by NotI digestion and cloned into the NotI site of the pBIN42 vector. This construct was transformed to *glr3.6b* single mutants for expression analysis and *glr3.3bglr3.6a* double mutants for complementation analysis. The GFP signal from this construct is visible using confocal microscopy but is not detectable under the imaging conditions used for Ca<sup>2+</sup> measurements, allowing it to be used in complementation assays with GCaMP Ca<sup>2+</sup> analysis.

All of the binary vectors were transformed into *Agrobacterium tumefaciens* strain GV3101 using electroporation. Arabidopsis plants were transformed using the floral dip methods (24). The primers used for cloning are detailed in Table S1.

### Real-time [Ca<sup>2+</sup>]<sub>cyt</sub> and [Glu]<sub>apo</sub> imaging in the entire plant

Arabidopsis plants expressing genetically-encoded  $\text{Ca}^{2+}$  and Glu indicators were imaged with a motorized fluorescence stereo microscope (SMZ-25, Nikon) equipped with a  $1\times$  objective lens (NA = 0.156, P2-SHR PLAN APO, Nikon) and a sCMOS camera (ORCA-Flash4.0 V2, Hamamatsu Photonics). The GFP-based  $\text{Ca}^{2+}$  indicator, GCaMP3, and Glu indicator, iGluSnFR, were excited using a mercury lamp (motorized Intensilight Hg Illuminator, Nikon), a 470/40 nm excitation filter, and a 500 nm dichroic mirror (P2-EFL GFP-B, Nikon). The green fluorescent signal passing through a 535/50 nm filter was acquired every 2 s with the sCMOS camera using NIS-Elements imaging software (Nikon).

For ratiometric  $\text{Ca}^{2+}$  imaging, the FRET-based  $\text{Ca}^{2+}$  indicator YCNano-65 was excited using a mercury lamp, a 436/20 nm excitation filter (ET436/20x, Chroma) and a 455 nm dichroic mirror (T455lp, Chroma). The fluorescence was separated by a 515 nm dichroic mirror (T515lp, Chroma) with image splitting optics (W-VIEW GEMINI, Hamamatsu Photonics) and the CFP (460-500 nm) and the cpVenus FRET (520-540 nm) signal passed independently through a 480/40 nm (ET480/40m, Chroma) and 535/30 nm filters (ET535/30m, Chroma), respectively. The resultant CFP and cpVenus (FRET) signals were simultaneously acquired every 2 s with the sCMOS camera using NIS-Elements imaging software. The FRET/CFP ratio was calculated and imaged by the 6D imaging and Ratio & FRET plug-in modules [Nikon; (25)].

To elicit wound responses, Arabidopsis rosette leaves are cut with scissors, crushed with a hemostat or fed on by larvae of the cabbage white butterfly (*Pieris rapae*; kindly provided by John Orrock, Department of Integrative Biology, University of Wisconsin, Madison).

Using the NIS-Elements imaging software, GCaMP3 and iGluSnFR signals were analysed over time at several regions of interest (ROIs), such as the wound site and petiole (For detail, see Fig. S4A). In order to calculate the fractional fluorescence changes ( $\Delta F/F$ ), the equation  $\Delta F/F = (F - F_0)/F_0$  was used, where  $F_0$  denotes the average baseline fluorescence determined by the average of  $F$  over the first 10 frames of the recording (26, 27) before the wounding/treatment.

#### Application of amino acids and chemical agents

Each of the 20 L-amino acids, D-Glu,  $\alpha$ -ketoglutarate and sorbitol were dissolved in growth medium [ $1/2\times$  MS salts, 1% (w/v) sucrose and 0.05% (w/v) MES; pH 5.1] to make a 100 mM stock solution (except for tyrosine and tryptophan where saturated solutions of approximately 2.5 and 50 mM respectively were used), and then 10  $\mu\text{l}$  was applied to a cut surface of leaf 1 after a 20 min recovery period after cutting the apical  $\sim 1\text{mm}$  from the leaf. We found this pre-cutting was necessary to allow reproducible access of the compounds to the leaf interior. This approach led to a reduction in the degree of subsequent wound-induced systemic gene induction when compared to non-pre-cut experiments but e.g., the level of systemic defense gene induction was statistically indistinguishable ( $P < 0.05$ ) between a cutting wound made to such pre-cut plants *JAZ5* (25.09 $\pm$ 8.24-fold), *JAZ7* (107.90 $\pm$ 61.33), *OPR3* (13.83 $\pm$ 2.56), *RBOHD* (3.48 $\pm$ 1.20) and *ZAT12* (3.48 $\pm$ 1.20) and the Glu treatment shown in Fig. 4 and S13. Oligogalacturonide (OG) pools with an average degree of polymerization of 5 to 15 were kind gifts from Toshihisa Kotake (Department of Biochemistry and Molecular Biology, Saitama University). OG and flg22 were dissolved into water to make a 400  $\mu\text{g}/\text{mL}$  and 10  $\mu\text{M}$  stock solution, respectively, and then 10  $\mu\text{l}$  was applied to the cut surface of leaf 1.  $\text{LaCl}_3$  was dissolved into 0.05% (v/v) Silwet L-77 in water to make a 50 mM stock solution and then 10  $\mu\text{l}$  was applied to a piece of Kimwipes (2-4 mm in width) placed on a petiole for 20 min prior to the experiment.

#### Confocal image analysis of GLR-EGFP

Hand sections of mature leaves and petioles from *glr3.3* mutants expressing *pGLR3.3::GLR3.3-EGFP* (15), a kind gift from Edgar Spalding (Department of Botany, University of Wisconsin, Madison), and *glr3.6* mutants expressing *pGLR3.6::GLR3.6-EGFP* were placed on a cover glass (24 × 50 mm, Fisher Scientific), immersed in a growth medium [1/2× MS salts, 1% (w/v) sucrose and 0.05% (w/v) MES; pH 5.1], and subsequently covered with a cover glass (18 × 18 mm, VWR International). Images of the GFP signal were acquired with a laser scanning confocal microscope (LSM780/Elyra; Zeiss). GFP was excited by a 488-nm laser/488-nm dichroic mirror, and fluorescent signal 510-560 nm was detected using the microscope's GaAsP detector.

#### iGluSnFR calibration *in vivo*

For iGluSnFR calibration in leaves, an edge (approximately 1 mm from the tip of leaf 1) was cut with scissors, allowed to recover for 30 mins and then 10 µl of solution [1/2× MS salts, 1% (w/v) sucrose and 0.05% (w/v) MES; pH 5.1] with different Glu concentrations (0, 0.0001, 0.001, 0.01, 0.1, 1, 10 and 100 mM) was applied to the cut edge. iGluSnFR signal was acquired at the cut site using the Nikon fluorescence stereo microscope and  $\Delta F/F$  was analysed. For iGluSnFR calibration in roots, the transgenic lines were grown under sterile conditions in a thin layer (~2 mm) of a growth medium [1× MS salts, 1% (w/v) sucrose, 0.5% (w/v) gellan gum and 0.05% (w/v) MES; pH 5.8] on a No. 1.5 cover glass (24 × 50 mm, Fisher Scientific) for 7 d under continuous light (90–100 µmol m<sup>-2</sup> s<sup>-1</sup>) at 22 °C. A small window (~500 µm × 500 µm) was excised from the gel exposing a region of the root situated at 5-10 mm from the root tip. This window in the gel allowed precise application of Glu and D-Sorbitol solutions of known concentration. iGluSnFR signal was acquired using the laser LSM 780 scanning confocal microscope and  $\Delta F/F$  was analysed.

#### Total RNA isolation, cDNA synthesis and quantitative PCR

For qPCR analysis, leaf 1 samples of wild type and the PDLP5 overexpression line were cut with scissors or treated with Glu or Sorbitol at the cut edge as described above. After the wounding/treatment, samples of leaves 5 and 6 were harvested at 0, 2, 5, 15, 30 60 and 180 min and rapidly frozen in liquid nitrogen.

Total RNA was extracted from flash-frozen leaf tissue (50–200 mg) using the RNeasy Plant Mini Kit (Qiagen) following the manufacturer's instructions. The samples were further treated by RNase-free DNase I to remove any residual genomic DNA using the TURBO DNase kit (Ambion) using the manufacturer's suggested protocols. First-strand cDNA was then synthesized from the total RNA (1–2 µg) in a 40-µL reaction (25–50 ng of total RNA per µL) with the SuperScript III First-Strand Synthesis System for RT-PCR (Invitrogen). In a 96-well optical PCR plate (ABgene), cDNA proportional to 10 ng of starting total RNA was combined with 200 nM of each primer (Table S1) and 7.5 µL of 2× EvaGreen qPCR master mixed with ROX passive reference dye (Biotium) to a final volume of 15 µL. Using the Arabidopsis *UBQ10* gene as an internal reference for standardization (28), qPCR analysis was performed using Mx3000P QPCR System as well as MxPro qPCR software (Agilent Technologies) with the following cycling parameters: 95°C for 15 min; 40 cycles of 95°C for 20 s, 58°C for 15 s, 65°C for 15 s; and then 1 cycle of dissociation from 58 to 95°C with 0.5°C increments. Expression of the marker genes was quantitated using the quantification cycle [C<sub>q</sub>; (29)].

#### Quantification of jasmonate content in leaf tissues

Metabolite extraction and quantification of JA and JA-Ile in leaf tissues were carried out according to previously described methods using ultra performance liquid chromatography electrospray ionization tandem mass spectrometry (ACUITY H-class, Xevo TQ-S, Waters)

(8) with minor modifications described in (30). Dihydro-JA (dhJA) and [ $^{13}\text{C}_6$ ]-JA-Ile were added to the extraction solvent [methanol:water:acetic acid = 70:29:0.5 (v/v/v)] as internal standards. Multiple reaction monitoring (MRM) was programmed to detect characteristic MS transitions for JA ( $m/z$ , 209 > 29), dhJA (211 > 59), JA-Ile (322 > 130), and [ $^{13}\text{C}_6$ ]-JA-Ile (328 > 136). MassLynx 4.1 and TargetLynx (Waters) were used to analyze the data. Calculations were based on calibration curves generated by known amounts of analytes and internal standards.

#### Statistical analysis

Quantitative measurement of GCaMP and iGluSnFR fluorescence, qPCR and LC/MS data were statistically analyzed by a two-way ANOVA followed by Bonferroni post-tests or Dunn's multiple comparison test using GraphPad Prism (GraphPad Software, Inc.). The velocities of  $\text{Ca}^{2+}$  wave was analyzed by t-test using GraphPad Prism using the criterion of a rise to 2x SD above pre-stimulation levels as a marker of a detectable increase in signal and dividing this timing by the linear distance from the wound site (31). We also used the criterion of a significant rise in signal above the pre-stimulated values as representing detection of a  $\text{Ca}^{2+}$  increase in assigning patterns of leaves showing  $\text{Ca}^{2+}$  increases in Table S1. Asterisks and different letters denote statistical differences (\*,  $P < 0.05$ ) between leaf 6 and 5, time 0 and other time points and wild type and mutants. All data are presented as mean  $\pm$  SE.

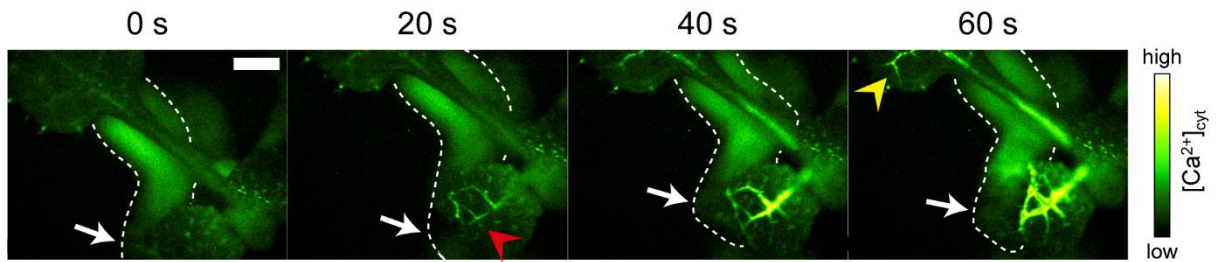


**Fig. S1. Long-distance  $[Ca^{2+}]_{cyt}$  increases move from young to older leaves in response to caterpillar herbivory.**

A caterpillar (outlined by white dashed line) feeding on the leaf (white arrow) caused a local  $[Ca^{2+}]_{cyt}$  increase (red arrowhead) that is propagated to distal older leaves (yellow arrowhead).  $Ca^{2+}$  levels monitored using transgenic reporter line expressing GCaMP3. Note that the caterpillar is naturally fluorescent and not expressing GCaMP. Scale bar, 1 mm.

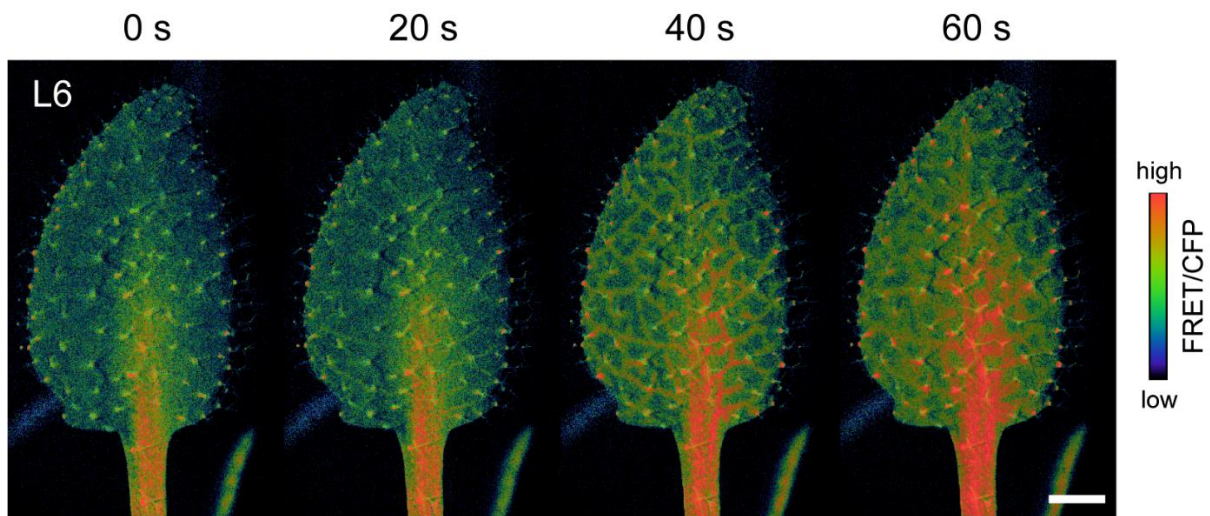


**Fig. S2. Wound-induced systemic spread of Ca<sup>2+</sup> increase monitored with YCNano-65.** Leaf 1 was wounded and Ca<sup>2+</sup> dynamics in leaf 6 followed using the ratiometric YCNano-65 Ca<sup>2+</sup> sensor. Time is after wounding leaf 1. Because single wavelength reporters such as GCaMP can yield imaging artifacts (32), we also validated the responses using plants expressing the Yellow Cameleon ratiometric GFP-based Ca<sup>2+</sup> sensor [YCNano-65; (31, 33)] which corrects for many of these potential issues. Unfortunately, the Cameleon sensors proved complex to use routinely in these low magnification imaging studies due to their smaller dynamic range whereas we and others [e.g., (26)] have found the single wavelength sensors well-suited to monitoring events at low magnifications, which focused our analysis on using GCaMP as our major imaging tool. Scale bar, 1 mm.

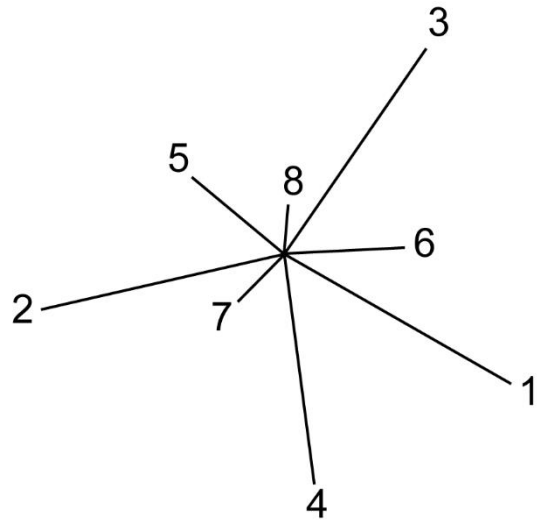
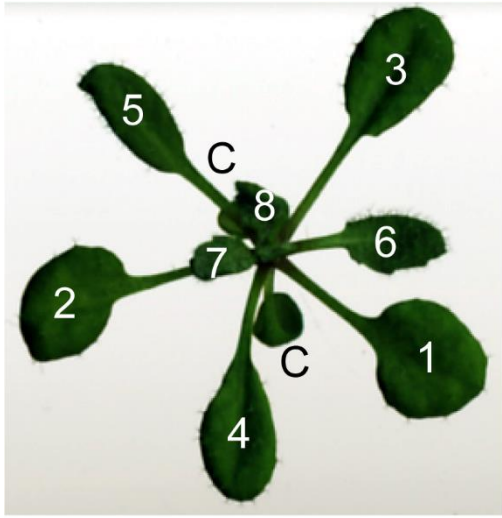


**Fig. S3. Numbering of leaves in the Arabidopsis rosette.** Leaves were numbered from oldest to youngest according to (3). C, cotyledons.

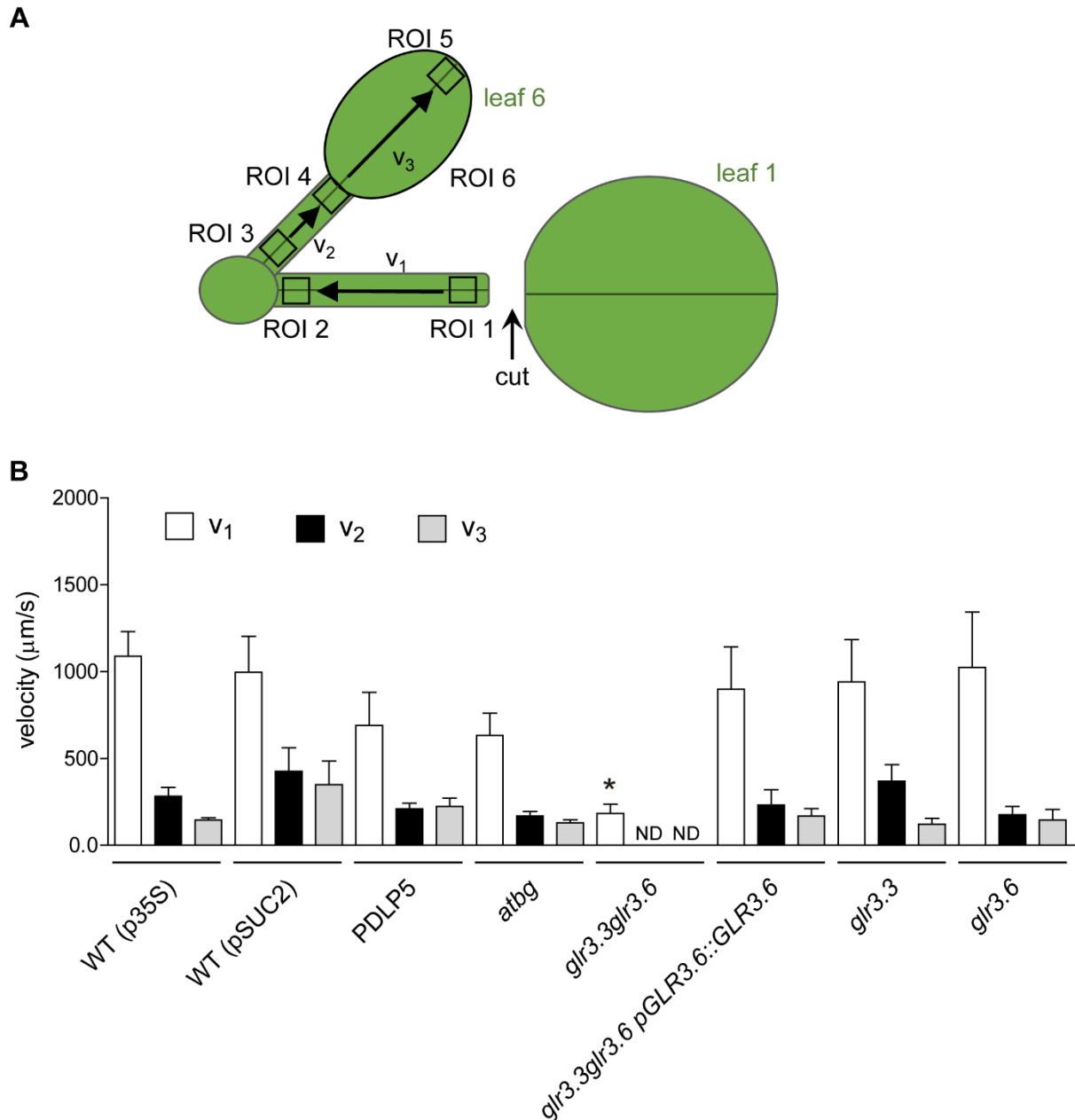


**Fig. S4. Velocities of the long-distance transmission of  $[Ca^{2+}]_{cyt}$  increase upon mechanical wounding.**

(A) Diagram showing Arabidopsis leaves and the regions of interest (ROI) used to analyze the  $[Ca^{2+}]_{cyt}$  changes and velocities ( $v_1$ - $v_3$ ) from the long-distance transmission of  $Ca^{2+}$  increases.  $v_1$  is between ROI 1 and 2 on the petiole of wounded leaf 1;  $v_2$  is between ROI 3 and 4 on the petiole of systemic leaf 6; and  $v_3$  is between ROI 4 and 5 on the blade of leaf 6. ROI 6 encompasses the entire leaf 6 blade. (B) Velocities ( $\mu\text{m/s}$ ) of the long-distance elevation in  $Ca^{2+}$  monitored using sensor expressing plants with GCaMP driven by the ubiquitously expressed p35S promoter in wild type (WT) and in plasmodesmatal and glutamate receptor mutant lines. In addition, WT expressing GCaMP driven by the phloem-specific pSUC2 promoter was analyzed. An asterisk denotes statistical differences (\*,  $P < 0.05$ ) from the WT (p35S) data. The increase in signal used to calculate velocity was defined as an increase to above 2 SD of the pre-stimulation levels (13). Error bars, mean  $\pm$  SE.  $N > 4$  replicates per line. ND, not detected.

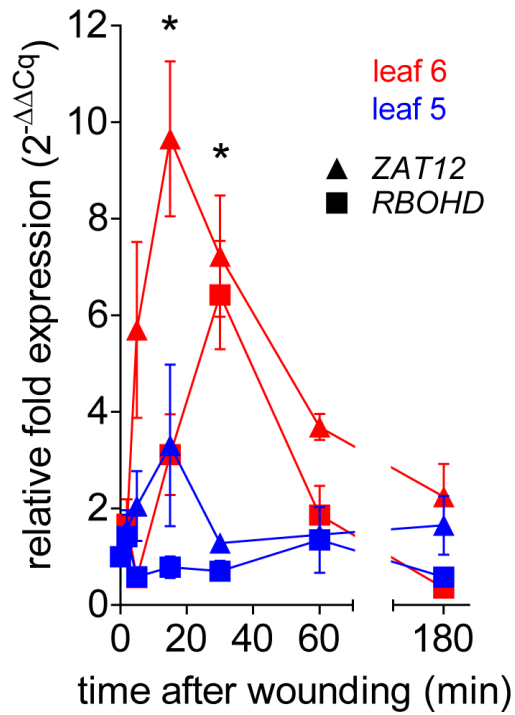


**Fig. S5 Systemic induction of defense response-related genes in leaf 6 after wounding leaf 1.**

Expression of *RBOHD* and *ZAT12* were assessed using qPCR in target leaf 6 and non-target leaf 5 after wounding of leaf 1. Error bars, mean  $\pm$  SE. \*,  $P < 0.05$ .  $N = 6$  replicates.

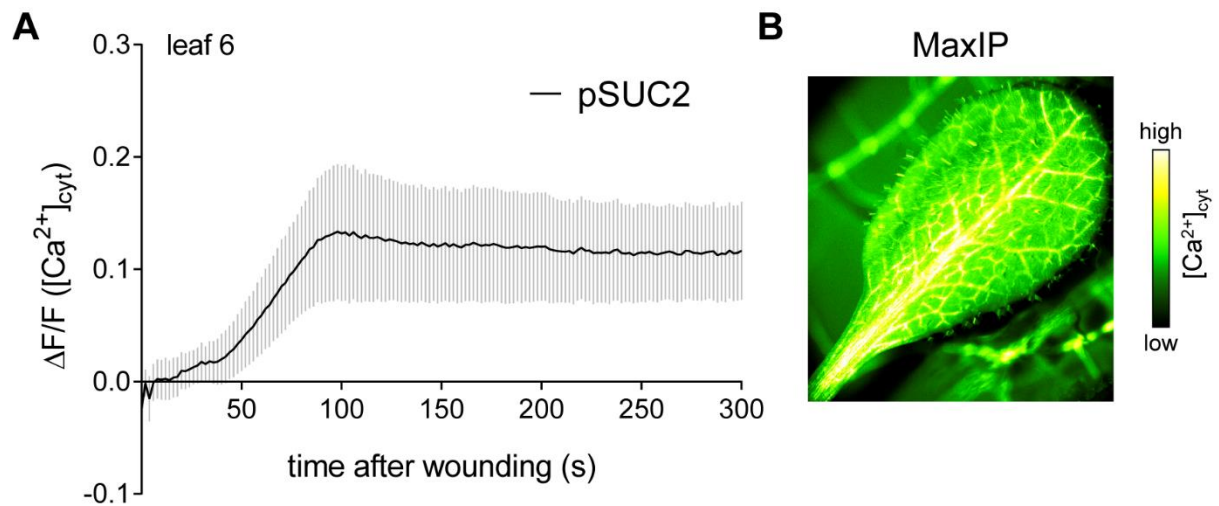


**Fig. S6. Wound-induced  $\text{Ca}^{2+}$  increase transmitted through the phloem.**

(A)  $[\text{Ca}^{2+}]_{\text{cyt}}$  levels in the phloem (sieve tube and companion cells) of the target leaf 6 after cutting leaf 1. Error bars, mean  $\pm$  SE.  $N = 3$  replicates. (B) Sum of images (MaxIP) in the target leaf 6 for 300 s after cutting leaf 1 showing extent of change.  $\text{Ca}^{2+}$  levels monitored selectively in the phloem using plants expressing GCaMP3 driven by the SUC2 promoter.

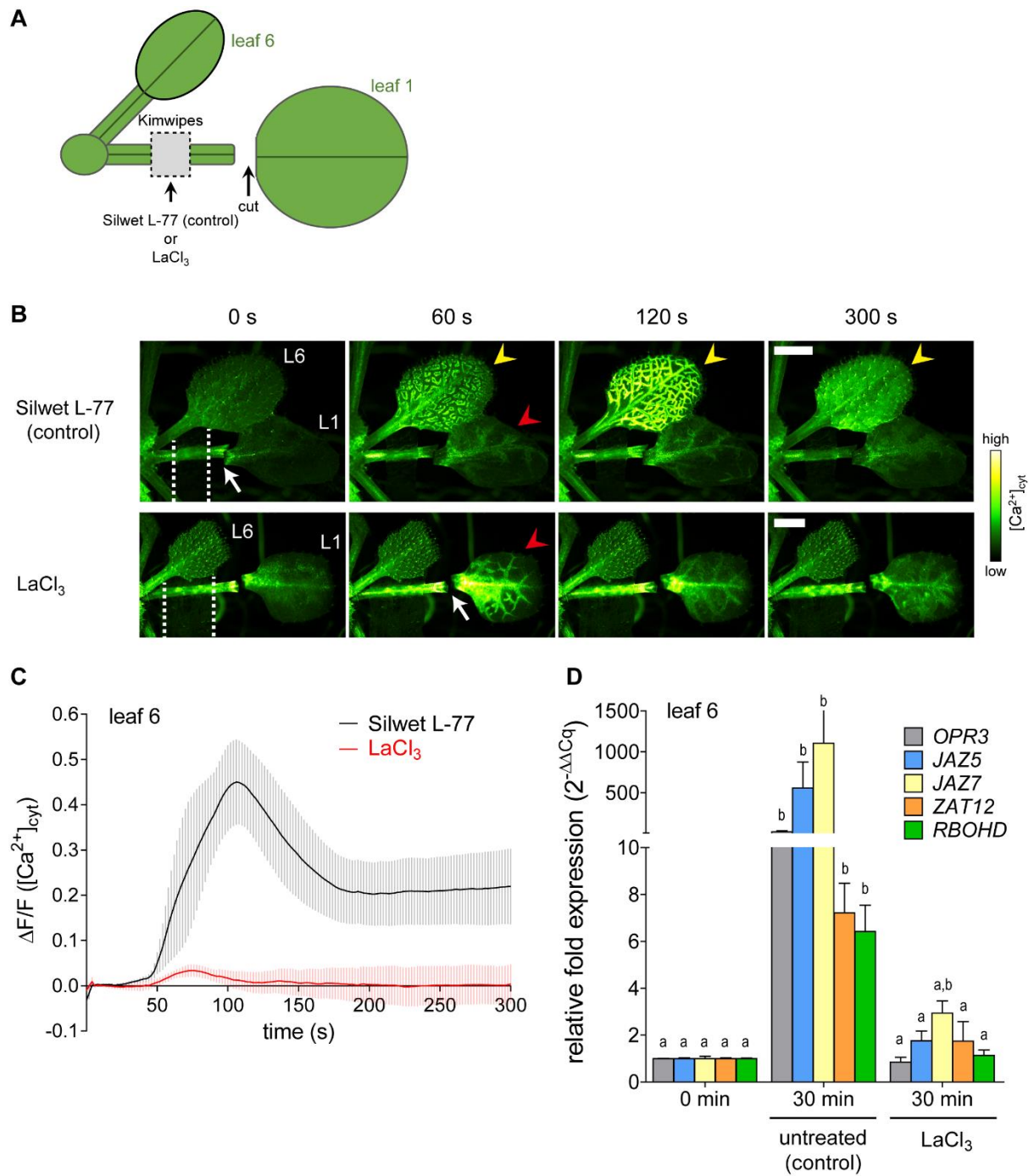


**Fig. S7 LaCl<sub>3</sub> blocks systemic [Ca<sup>2+</sup>]<sub>cyt</sub> increases and wound-induced defense gene induction.**

(A) The Ca<sup>2+</sup> channel blocker LaCl<sub>3</sub> (50 mM) was added to a strip of Kimwipes laid over the petiole of the leaf 1 (L1). 0.05% (v/v) Silwet was added as a wetting agent to improve LaCl<sub>3</sub> penetration of the cuticle. (B-D) [Ca<sup>2+</sup>]<sub>cyt</sub> (B, C) and defense marker gene induction (D) were then monitored with GCaMP3 and qPCR respectively in leaf 6 (L6) as L1 was wounded by cutting. Note that LaCl<sub>3</sub> treatment blocked systemic propagation of the increase in [Ca<sup>2+</sup>]<sub>cyt</sub> to L6 and attenuated wound-responsive gene induction in this systemic tissue. Error bars, mean ± SE. *N* > 4 replicates (C, D). Different letters denote statistical differences (*P* < 0.05).

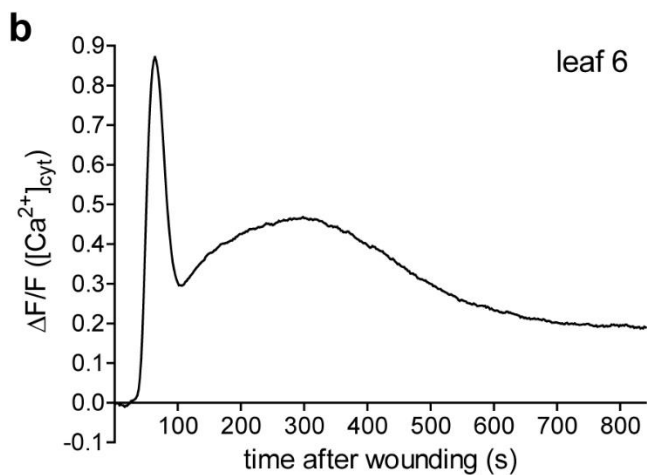
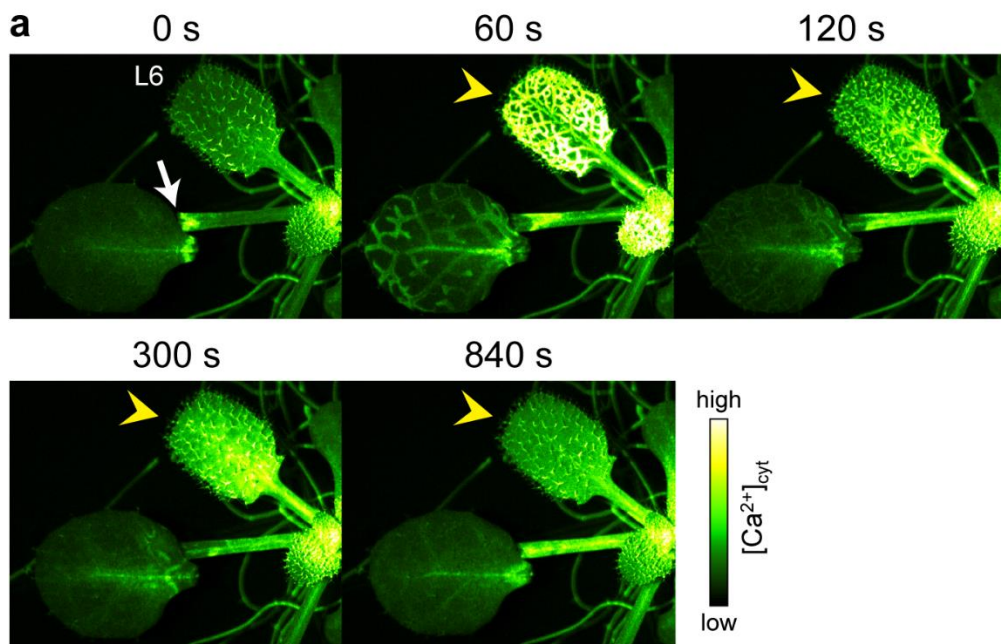


**Fig. S8. Long-term imaging of the transmission of the  $\text{Ca}^{2+}$  increase after mechanical wounding.**

(A) Cutting the leaf 1 blade-petiole junction (white arrow, 0 s) caused a  $[\text{Ca}^{2+}]_{\text{cyt}}$  increase in leaf 6 (L6) that lasted over 14 min. (B) The biphasic  $[\text{Ca}^{2+}]_{\text{cyt}}$  signature in leaf 6 (yellow arrow) upon distal mechanical wounding.  $\text{Ca}^{2+}$  levels monitored using transgenic reporter line expressing GCaMP3.

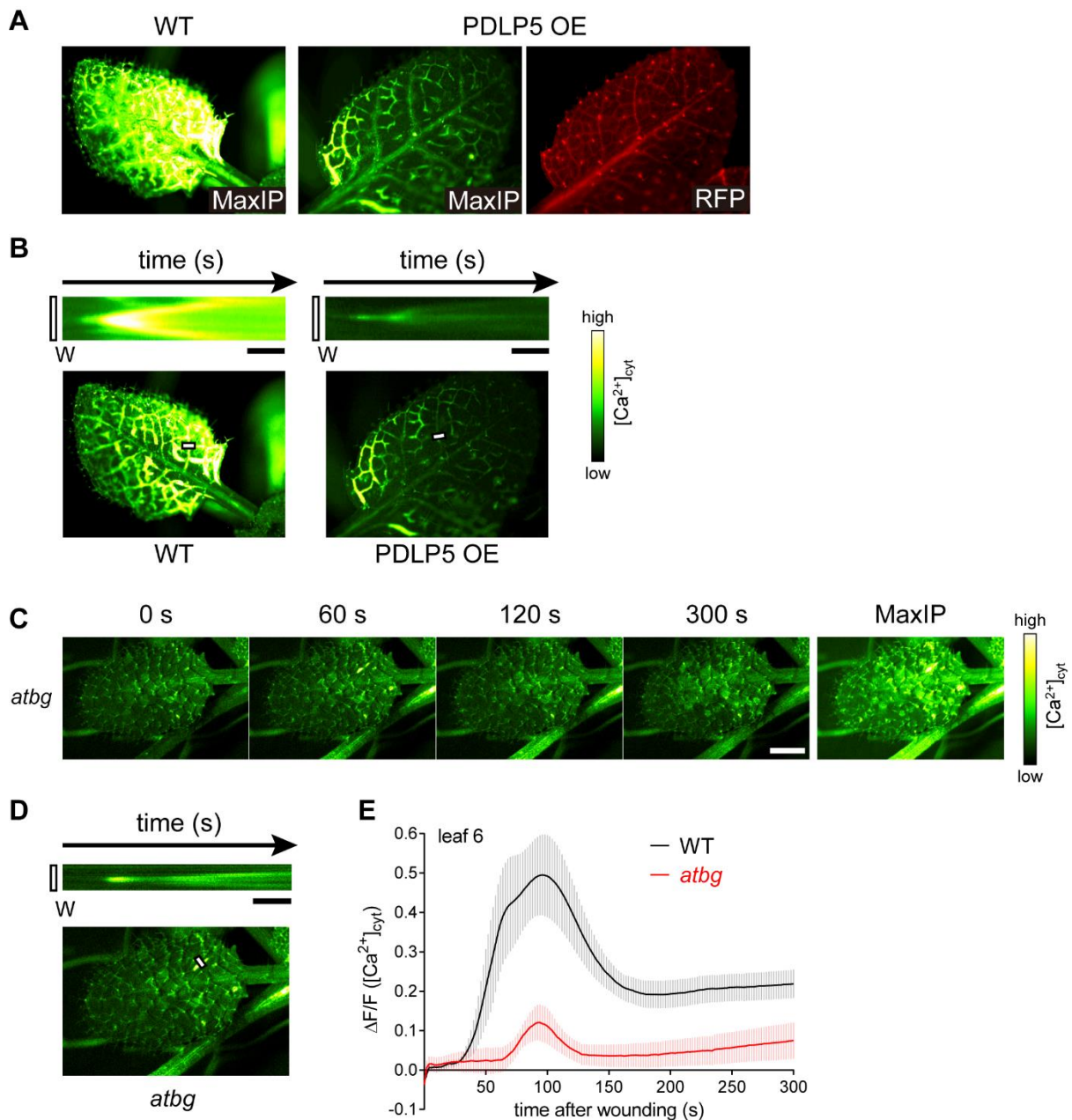


**Fig. S9. Spatially-restricted spread of Ca<sup>2+</sup> increases in the target leaf 6 of *PDL5 OE* and *atbg* mutant.**

(A) Sum of images (MaxIP) in the target leaf 6 for 300 s after cutting leaf 1 showing extent of change in wild type and the *PDL5 OE* line. The red (RFP) channel shows the expression pattern of *PDL5-RFP*. (B) Kymograph data in wild type and *PDL5 OE*. The white bar on the leaf images indicates a 0.25 mm line where GCaMP intensity data was extracted and is reproduced to the left of each kymograph to help orient the graph to the leaf region it represents. These kymographs show data for each time point in the analysis (every 2 sec) plotted sequentially along the time axis. W (wounding) denotes the time 0 from when leaf 1 was cut. The total duration of each kymograph is 300 s. Time scale bar, 50 s. (C) Snapshots of Ca<sup>2+</sup> changes and sum of images (MaxIP) in the target leaf 6 for 300 s after cutting leaf 1 showing extent of change in the *atbg* mutant. Scale bar, 1 mm. (D) Kymograph data by line as described above. Time scale bar, 50 s. (E) [Ca<sup>2+</sup>]<sub>cyt</sub> signature in leaf 6 upon wounding in wild type and *atbg* mutants. Scale bar, 1 mm. Error bars, mean ± SE. *N* > 7 replicates.

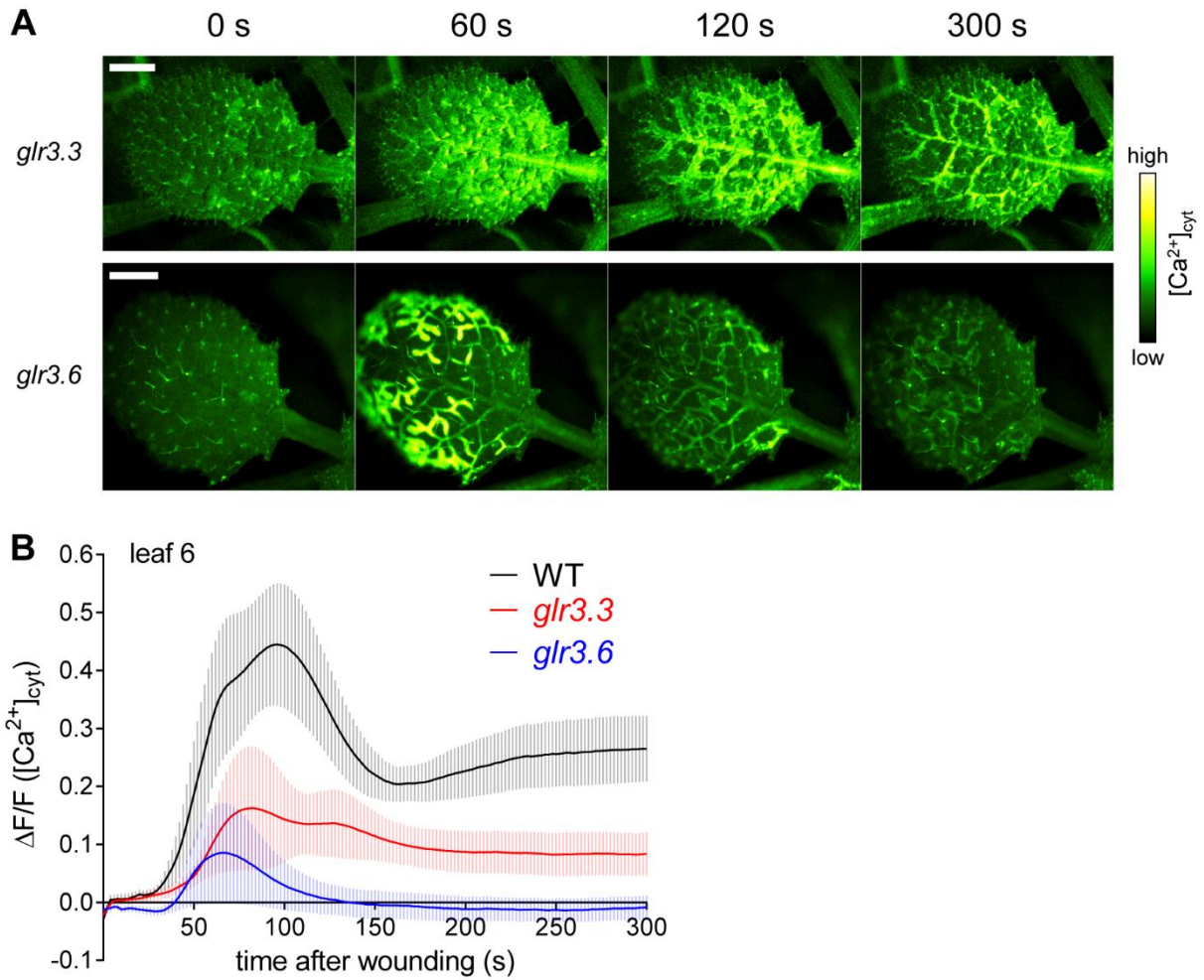


**Fig. S10. Long-distance transmission of [Ca<sup>2+</sup>]<sub>cyt</sub> changes in *glr3.3* and *glr3.6* single mutants.**

(A) Reduced [Ca<sup>2+</sup>]<sub>cyt</sub> increases in leaf 6 of *glr3.3* and *glr3.6* single mutants after cutting leaf 1 (0 s). Scale bar, 1 mm. (B) [Ca<sup>2+</sup>]<sub>cyt</sub> signature in leaf 6 upon mechanical wounding in wild type and *glr3.3* and *glr3.6* mutants. Error bars, mean ± SE. *N* > 8 replicates. WT data is reproduced from Fig. 1 to aid in comparison. Note that the differential effects of the individual *glr* mutants on systemic Ca<sup>2+</sup> increases may reflect these channels acting to support independent, parallel components of the response, providing an explanation of why a double knockout is required to ablate the entire response.

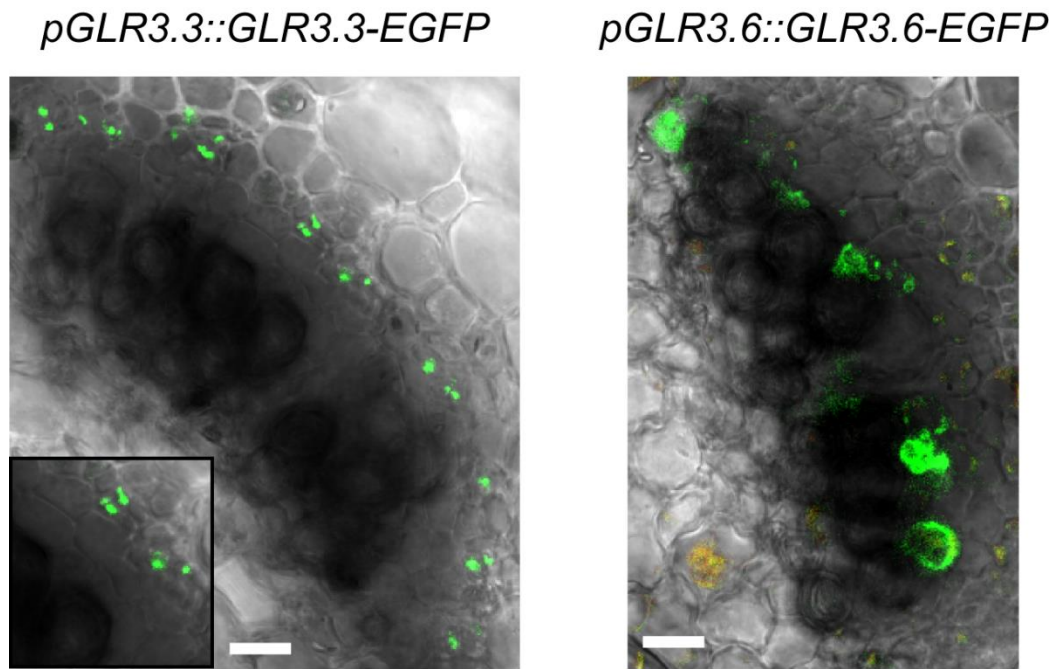


**Fig. S11. Protein expression patterns of GLR3.3 and GLR3.6.**

Transverse section of petiole of plants expressing *pGLR3.3::GLR3.3-EGFP* or *pGLR3.6::GLR3.6-EGFP*. Note the accumulation of GFP signal in phloem for GLR3.3-EGFP and xylem contact cells for GLR3.6-EGFP. Scale bar, 10 mm.



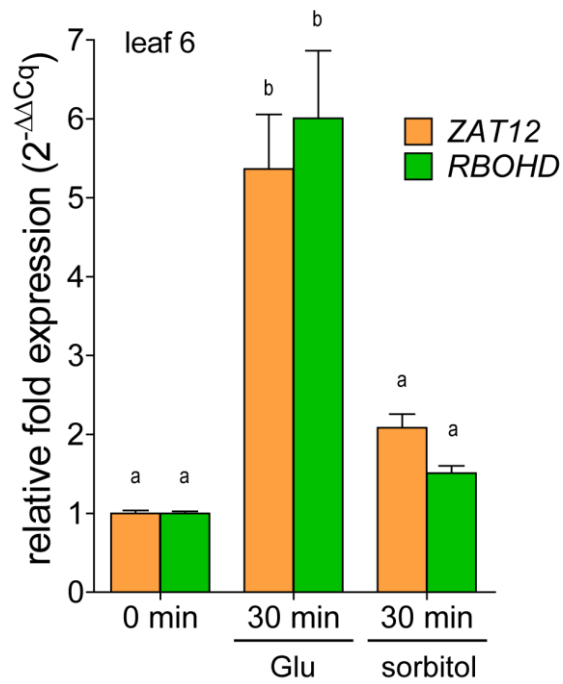


**Fig. S13 Systemic induction of defense response-related genes in leaf 6 upon Glu treatment to leaf 1.**

Expression of *RBOHD* and *ZAT12* were assessed using qPCR in target leaf 6 after treatment of leaf 1 with either 100 mM Glu or 100 mM sorbitol (control). Note significant induction of transcripts in Leaf 6 upon Glu treatment of Leaf 1. Error bars, mean  $\pm$  SE.  $N > 4$  replicates. Different letters denote statistical differences ( $P < 0.05$ ).

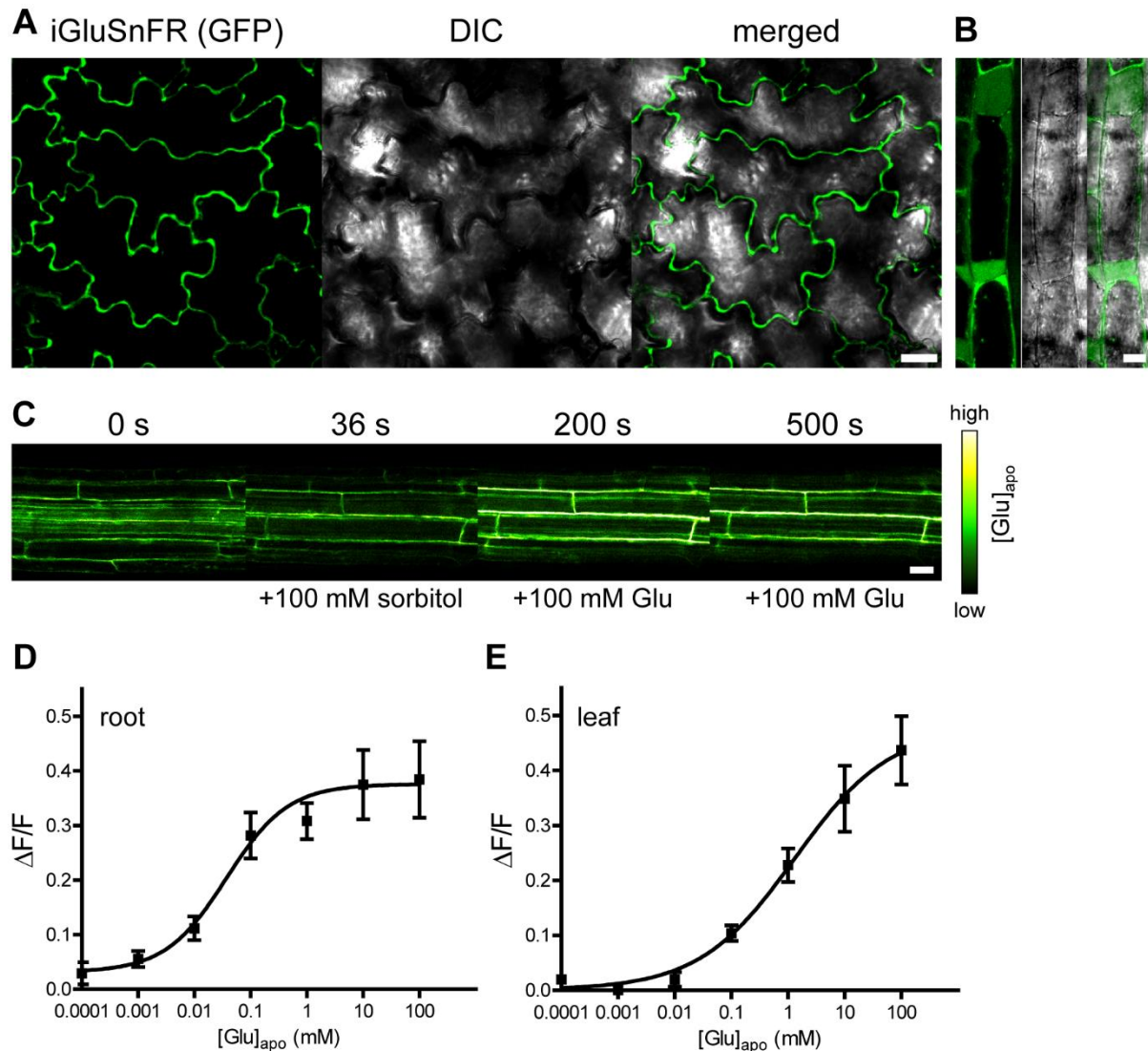


**Fig. S14. Characterization of the GFP-based Glu sensor iGluSnFR targeted to the apoplast.**

(A, B) Localization of the iGluSnFR signal in the cell wall of leaf epidermal cells (A) and hypocotyl epidermal cells (B) after plasmolysis with 1 M sorbitol for 30 min to confirm the cell wall localization of the sensor. Note that GFP signal still resides in cell wall even after the protoplast has shrunk away from the wall due to the plasmolysis. (C) Application of 100 mM Glu (200 s), but not sorbitol (36 s), causes an elevation of the iGluSnFR signal in the root epidermal cells. Note, this is the same root treated sequentially with sorbitol at ~34 s and then Glu at ~198 s. An instantaneous change in iGluSnFR signal is seen in response to Glu but not sorbitol. The 36 s image is reflective of the lack of response seen throughout the subsequent sorbitol treatment period until Glu addition. (D, E) Dose-dependency of the iGluSnFR signal in roots (D) and leaves (E), see methods for protocol for applying Glu to the iGluSnFR expressing leaves. Error bars, mean  $\pm$  SE.  $N > 3$  replicates. Scale bar, 20  $\mu$ m.

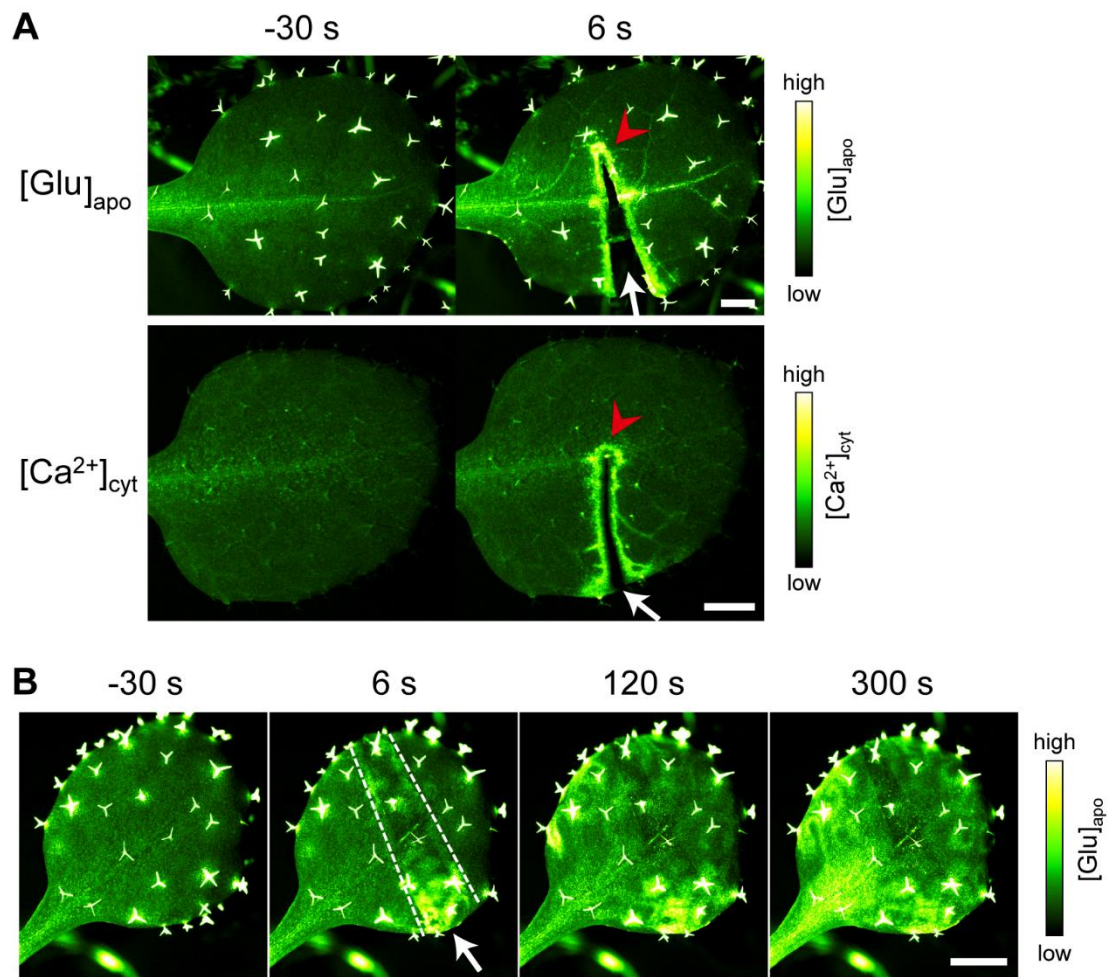


**Fig. S15. Elevations of the apoplastic iGluSnFR signal in response to cutting and crushing.**

(A) Cutting the leaf 1 with scissors (white arrow) caused a rapid, local  $[Glu]_{apo}$  elevation (red arrow in the upper panel) which is spatially correlated with a rapid, local  $[Ca^{2+}]_{cyt}$  increase in the wounded leaf (red arrow in the lower panel). (B) Crushing the leaf 1 with a hemostat (white arrow/dashed line, 0 s) caused an increase in  $[Glu]_{apo}$  that spreads throughout the crushed leaf. Scale bars, 1 mm.

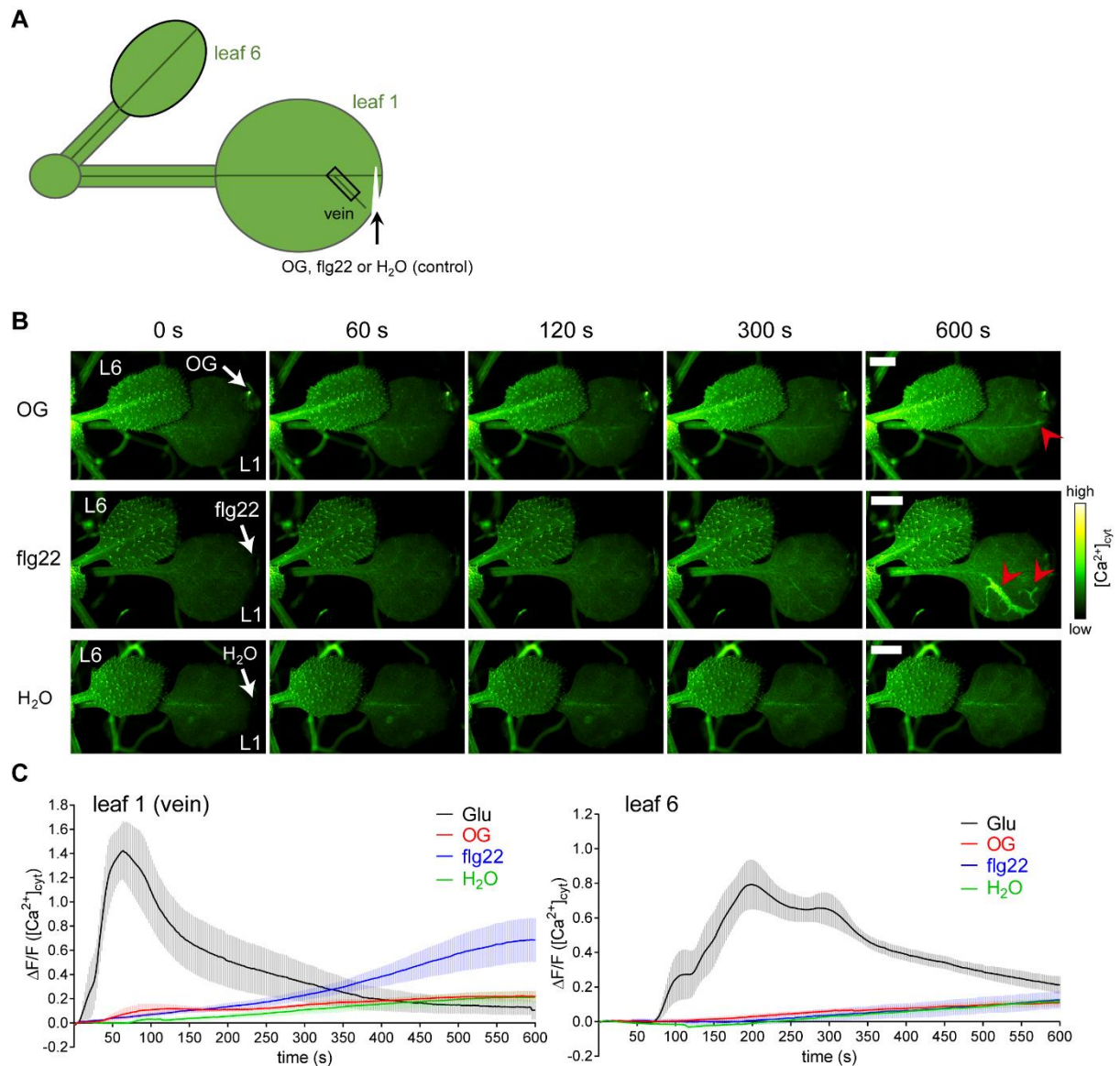


**Fig. S16. Oligogalacturonides and flg22 fail to elicit rapid systemic  $[Ca^{2+}]_{cyt}$  increases.** (A-C) 400  $\mu\text{g}/\text{mL}$  oligogalacturonide (OG) and 10  $\mu\text{M}$  flg22 were added to leaves as for previous Glu treatments. Although both OG and flg22, but not the water control, caused local  $[Ca^{2+}]_{cyt}$  increases within the treated leaf (red arrowheads, B, C), no propagating systemic  $Ca^{2+}$  increases to leaf 6 were detectable (C), whereas 100 mM Glu under the same conditions led to an easily detected systemic response (C). Error bars, mean  $\pm$  SE.  $N > 5$  replicates. Scale bar, 2 mm.

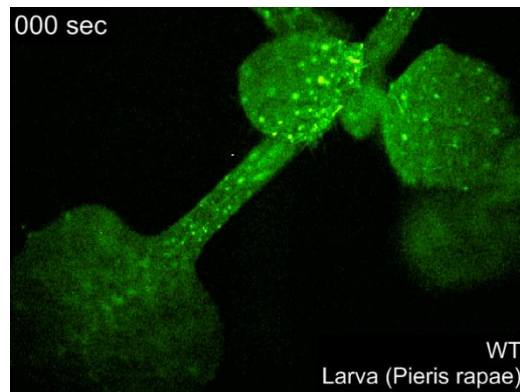
**Table S1. Percentage of times systemic leaves at each position within the rosette showed an increased  $[Ca^{2+}]_{cyt}$  upon mechanical wounding of a different leaf.**

Response <sup>1</sup> Wounded <sup>2</sup>	Leaf 1	Leaf 2	Leaf 3	Leaf 4	Leaf 5	Leaf 6	Leaf 7	Leaf 8
Cut leaf 1	×	0%	74% <sup>3,4</sup>	43%	0%	87%	0%	9%
Cut leaf 2	0%	×	5%	21%	95%	0%	47%	21%
Cut leaf 3	35%	12%	×	12%	24%	82%	0%	41%
Cut leaf 4	67%	17%	17%	×	11%	28%	33%	0%
Cut leaf 5	7%	87%	13%	0%	×	0%	73%	87%
Cut leaf 6	94%	0%	50%	25%	0%	×	0%	13%
Cut leaf 7	15%	65%	0%	60%	55%	0%	×	20%
Crushed leaf 1	×	93%	100%	86%	93%	100%	29%	57%

<sup>1</sup>Leaves monitored for a significant increase in  $[Ca^{2+}]_{cyt}$ . <sup>2</sup>Position of leaf mechanically wounded by cutting or crushing. <sup>3</sup>Percentage of cases of  $[Ca^{2+}]_{cyt}$  response (defined as a significant increase in distal leaf  $[Ca^{2+}]_{cyt}$  above its pre-stimulus signal) calculated from  $N \geq 12$  per wounding pattern. <sup>4</sup> $n \pm 3$  and  $n \pm 5$  relationships coded (brown) and  $n \pm 2$  (blue). These patterns mirror the closest vascular inter-connections between Arabidopsis leaves that are established as the leaves sequentially initiate during develop (34). Note, setting a threshold of 33% of leaves responding, the major pattern of induction of systemic  $[Ca^{2+}]_{cyt}$  increase follows an  $n \pm 3$  and  $n \pm 5$  from the wounded leaf, except in the case of crushing where response throughout the rosette is evident. Occasionally an  $n \pm 2$  pattern is observed (leaf 7 to 5) likely reflecting the short vascular pathway known to exist from leaf 5 to 2 and then 2 to 7 (34). Such a prominent role for patterns of vascular connectivity is also seen in the patterns of systemic wound-induced gene induction in e.g., poplar (35).

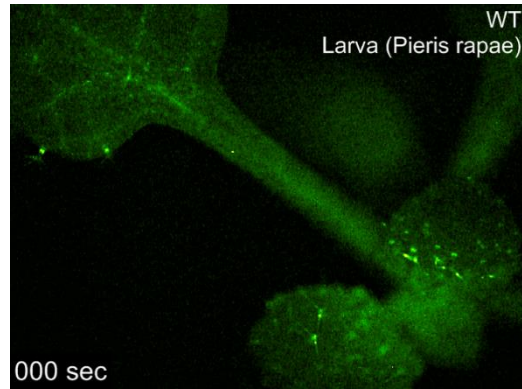
**Table S2. List of primers used in this study.**

For cloning	
Primer name	5' to 3'
GCaMP3(XbaI)_F	GCTCTAGACGCCACCATGGGTTCTCATCAT
GCaMP3(BamHI)_R	CGCGGATCCTTACTTCGCTGTCATCATTTGT
pSUC2(HindIII)_F	CGATAAGCTTAAGTTACTTTCTATTATTAAGTGTATAATGG
pSUC2(XbaI)_R	CGTCTAGAATTTGACAAACCAAGAAAGTAAGAAAAAAAAAG
basic	
chitinase_F(XbaI)	TATTCTAGAAACAATGAAGACTAATCTTTTTCTC
basic	
chitinase_R(BamHI)	ATAGGATCCGAATTCGGCCGAGGATAATGATAGGAG
iGluSnFR_F(BamHI)	ATTGGATCCATGGCCGCAGGCAGCACGCTGGAC
iGluSnFR_F(SmaI)	ATACCCGGGTTATTTCAAGTGCCTTGTCATTTCG
pGLR3.6_F(SphI)	CTTGTCATGCTTCCAGATTCCGATCAAAAGC
pGLR3.6_R(XbaI)	AATTCTAGACTTCTCAATTTCAAGGAGATTCC
GLR3.6_F(XbaI)	AATTCTAGAATGAAGTGGTTTCTGCTTATGC
GLR3.6_F(SmaI)	ATACCCGGGGTTGCAGCGACTTGAACCATTTCG
EGFP_F(SmaI)	TTACCCGGGGCTGCTGCCGCTGCCGCTGC
EGFP_R(SacI)	TTAGAGCTCTTACTTGTACAGCTCGTCCATG
For qPCR	
Primer name	5' to 3'
AtUBQ10-qPCR-F	CACACTCCACTTGGTCTTGCGT
AtUBQ10-qPCR-R	TGGTCTTTCCGGTGAGAGTCTTCA
OPR3-qPCR-For	CGTTTTACTCAAGATCCAGTTG
OPR3-qPCR-Rev	ATTATCAAACCTCAGAGGCGGG
JAZ5_qPCR-F1	TCATCGTTATCCTCCCAAGC
JAZ5_qPCR-R1	CACCGTCTGATTTGATATGGG
JAZ7_qPCR-F2	GATCCTCCAACAATCCCAA
JAZ7_qPCR-R2	TGGTAAGGGGAAGTTGCTTG
Zat12-qPCR-F(b)	TCATCAGAAGAAAAATGGTTGCG
Zat12-qPCR-R	AAGCATCAAACAATTCGCCG
RbohD_qPCR-F1	CCACGTTTAATTGCCGCG
RbohD_qPCR-R1	GCTAGTCGGTTGATCCCCAAA



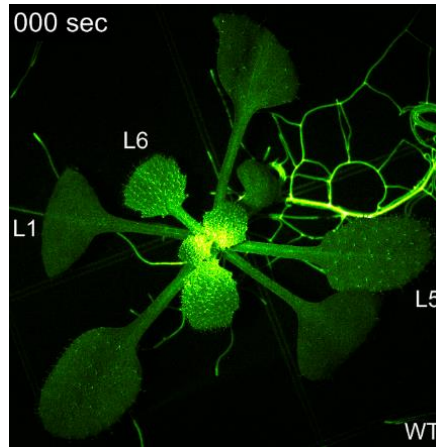
**Movie S1.**

Herbivory by larva of *Pieris rapae* on older Arabidopsis leaf showing Ca<sup>2+</sup> increases transmitted to younger leaves. Ca<sup>2+</sup> levels visualized using plants expressing GCaMP3. Note, the larva is naturally autofluorescent and signal from the caterpillar does not indicate information on Ca<sup>2+</sup> levels.



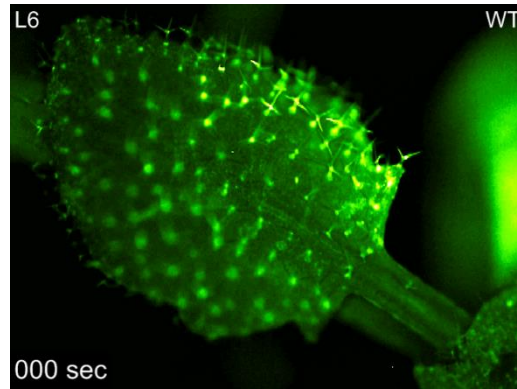
**Movie S2.**

Herbivory by larva of *Pieris rapae* on younger Arabidopsis leaf showing  $\text{Ca}^{2+}$  increases transmitted to older leaves.  $\text{Ca}^{2+}$  levels visualized using plants expressing GCaMP3. Note, the larva is naturally autofluorescent and signal from the caterpillar does not indicate information on  $\text{Ca}^{2+}$  levels.



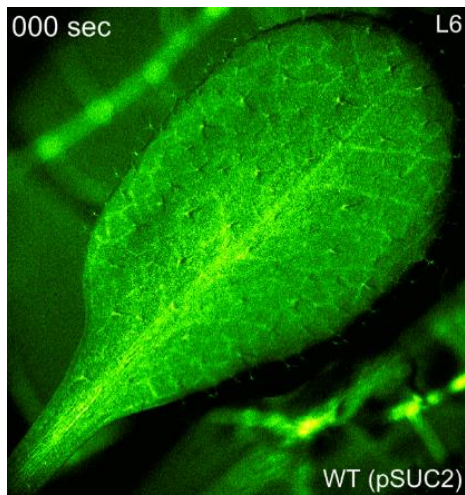
**Movie S3.**

Mechanical wounding (scissors) at the petiole of leaf 1 (L1) in wild-type plant showing Ca<sup>2+</sup> increases transmitted to target leaves [e.g., leaf 6 (L6)]. Ca<sup>2+</sup> levels visualized using plants expressing GCaMP3.



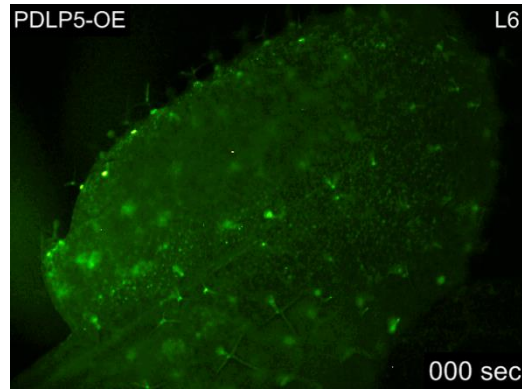
**Movie S4.**

Systemic Ca<sup>2+</sup> increase response in leaf 6 to mechanical wounding (scissors) at the petiole of leaf 1. Note rapid transmission of response through the vasculature and slower phase as the Ca<sup>2+</sup> increase spreads across the leaf blade. Ca<sup>2+</sup> levels visualized using plants expressing GCaMP3.



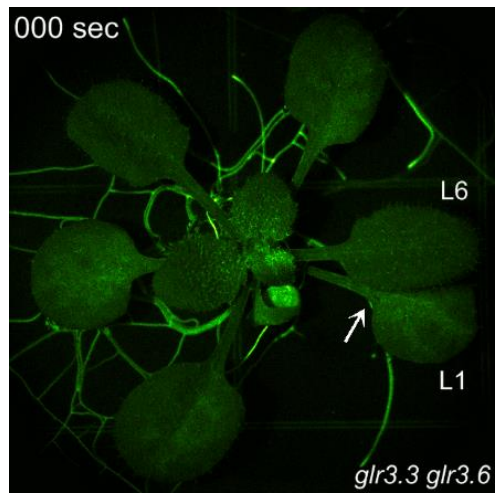
**Movie S5.**

Phloem localization of the systemic  $\text{Ca}^{2+}$  increase response in leaf 6 to mechanical wounding (scissors) at the petiole of leaf 1.  $\text{Ca}^{2+}$  levels visualized using plants expressing GCaMP3 driven by the pSUC2 promoter that localizes expression to the phloem sieve tube elements and companion cells.



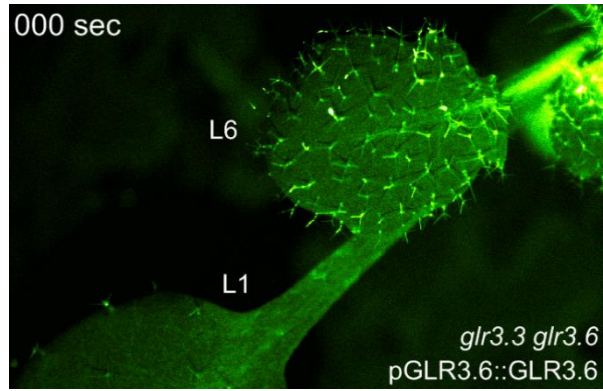
**Movie S6.**

Systemic  $\text{Ca}^{2+}$  increase response in leaf 6 to mechanical wounding (scissors) at the petiole of leaf 1 in a PDLP5 OE line. Note rapid transmission of response through the vasculature but lack of the slower phase of  $\text{Ca}^{2+}$  increase that normally spreads across the leaf blade from the leaf veins.  $\text{Ca}^{2+}$  levels visualized using plants expressing GCaMP3.



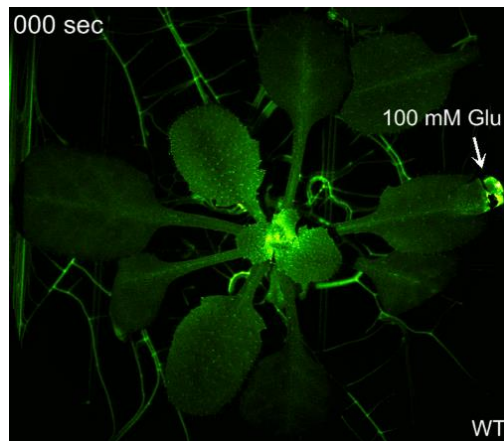
**Movie S7.**

Mechanical wounding (scissors) at the petiole of leaf 1 (L1) of the *glr3.3glr3.6* mutant showing a local  $[Ca^{2+}]_{cyt}$  increase that fails to be transmitted to systemic leaves such as leaf 6 (L6).  $Ca^{2+}$  levels visualized using plants expressing GCaMP3.



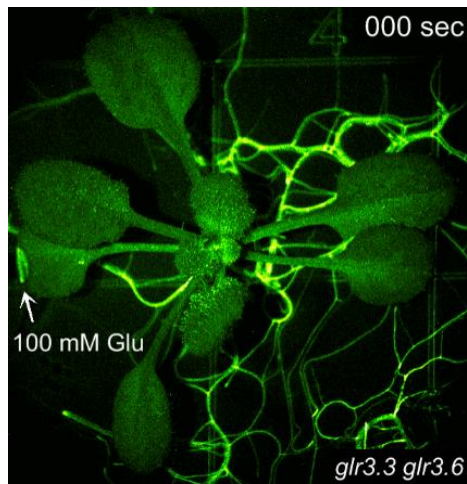
**Movie S8.**

Mechanical wounding (scissors) at the petiole of leaf 1 of the *glr3.3/glr3.6* mutant expressing *GLR3.6* driven by its native promoter showing restoration of the systemic transmission of  $[Ca^{2+}]_{cyt}$  increases from leaf 1 (L1) to leaf 6 (L6).  $Ca^{2+}$  levels visualized using plants expressing GCaMP3.



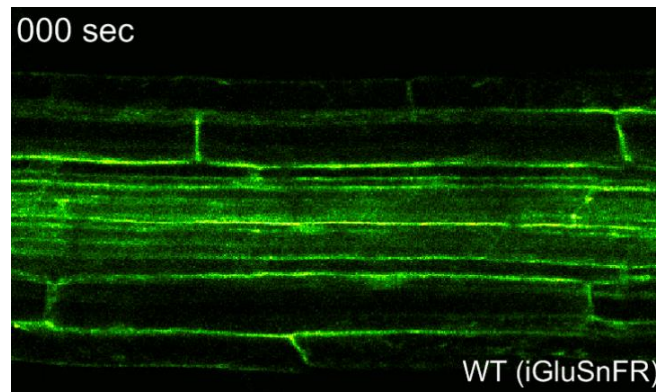
**Movie S9.**

Systemic transmission of  $[Ca^{2+}]_{cyt}$  elevation in wild-type Arabidopsis in response to 100 mM L-Glu added to the cut tip of a leaf.  $Ca^{2+}$  levels visualized using plants expressing GCaMP3.



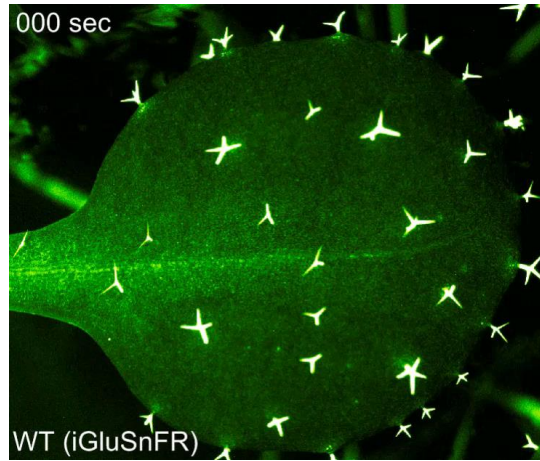
**Movie S10.**

Systemic transmission of Ca<sup>2+</sup> elevation in the *glr3.3glr3.6* double mutant in response to 100 mM L-Glu added to the cut tip of a leaf. Ca<sup>2+</sup> levels visualized using plants expressing GCaMP3.



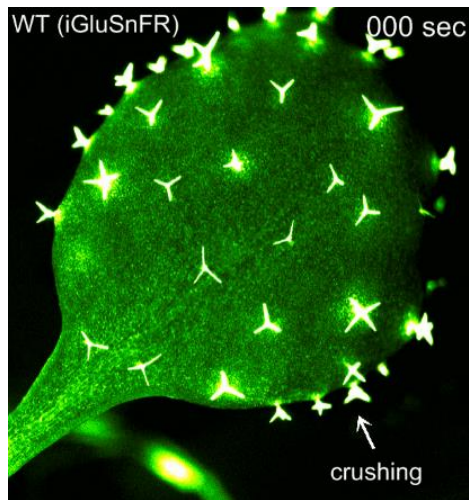
**Movie S11.**

Cell wall Glu in the root in response to sequential addition of 100 mM sorbitol and then L-Glu. Glu was monitored by iGluSnFR targeted to the cell wall using the chitinase signal sequence. Note increase in fluorescence in response to Glu but not sorbitol.



**Movie S12.**

Cell wall Glu in the leaf in response to mechanical wounding by cutting. Glu was monitored by iGluSnFR targeted to the cell wall using the chitinase signal sequence. Note increase in fluorescence around wound site and local vasculature.



**Movie S13.**

Cell wall Glu in the leaf in response to mechanical wounding by crushing using forceps. Glu was monitored by iGluSnFR targeted to the cell wall using the chitinase signal sequence. Note increase in fluorescence around wound site and then more broad spread over the leaf.

## References and Notes

1. G. A. Howe, I. T. Major, A. J. Koo, Modularity in jasmonate signaling for multistress resilience. *Annu. Rev. Plant Biol.* **69**, 387–415 (2018). [doi:10.1146/annurev-arplant-042817-040047](https://doi.org/10.1146/annurev-arplant-042817-040047) [Medline](#)
2. W. G. Choi, G. Miller, I. Wallace, J. Harper, R. Mittler, S. Gilroy, Orchestrating rapid long-distance signaling in plants with Ca<sup>2+</sup>, ROS and electrical signals. *Plant J.* **90**, 698–707 (2017). [doi:10.1111/tpj.13492](https://doi.org/10.1111/tpj.13492) [Medline](#)
3. S. A. Mousavi, A. Chauvin, F. Pascaud, S. Kellenberger, E. E. Farmer, GLUTAMATE RECEPTOR-LIKE genes mediate leaf-to-leaf wound signalling. *Nature* **500**, 422–426 (2013). [doi:10.1038/nature12478](https://doi.org/10.1038/nature12478) [Medline](#)
4. V. Salvador-Recatalà, W. F. Tjallingii, E. E. Farmer, Real-time, *in vivo* intracellular recordings of caterpillar-induced depolarization waves in sieve elements using aphid electrodes. *New Phytol.* **203**, 674–684 (2014). [doi:10.1111/nph.12807](https://doi.org/10.1111/nph.12807) [Medline](#)
5. V. Salvador-Recatalà, New roles for the GLUTAMATE RECEPTOR-LIKE 3.3, 3.5, and 3.6 genes as on/off switches of wound-induced systemic electrical signals. *Plant Signal. Behav.* **11**, e1161879 (2016). [doi:10.1080/15592324.2016.1161879](https://doi.org/10.1080/15592324.2016.1161879) [Medline](#)
6. B. G. Forde, M. R. Roberts, Glutamate receptor-like channels in plants: A role as amino acid sensors in plant defence? *F1000Prime Rep.* **6**, 37 (2014). [doi:10.12703/P6-37](https://doi.org/10.12703/P6-37) [Medline](#)
7. L. Tian, S. A. Hires, T. Mao, D. Huber, M. E. Chiappe, S. H. Chalasani, L. Petreanu, J. Akerboom, S. A. McKinney, E. R. Schreiter, C. I. Bargmann, V. Jayaraman, K. Svoboda, L. L. Looger, Imaging neural activity in worms, flies and mice with improved GCaMP calcium indicators. *Nat. Methods* **6**, 875–881 (2009). [doi:10.1038/nmeth.1398](https://doi.org/10.1038/nmeth.1398) [Medline](#)
8. A. J. Koo, X. Gao, A. Daniel Jones, G. A. Howe, A rapid wound signal activates the systemic synthesis of bioactive jasmonates in Arabidopsis. *Plant J.* **59**, 974–986 (2009). [doi:10.1111/j.1365-313X.2009.03924.x](https://doi.org/10.1111/j.1365-313X.2009.03924.x) [Medline](#)
9. G. Glauser, L. Dubugnon, S. A. R. Mousavi, S. Rudaz, J.-L. Wolfender, E. E. Farmer, Velocity estimates for signal propagation leading to systemic jasmonic acid accumulation in wounded Arabidopsis. *J. Biol. Chem.* **284**, 34506–34513 (2009). [doi:10.1074/jbc.M109.061432](https://doi.org/10.1074/jbc.M109.061432) [Medline](#)
10. W. J. Lucas, A. Groover, R. Lichtenberger, K. Furuta, S.-R. Yadav, Y. Helariutta, X.-Q. He, H. Fukuda, J. Kang, S. M. Brady, J. W. Patrick, J. Sperry, A. Yoshida, A.-F. López-Millán, M. A. Grusak, P. Kachroo, The plant vascular system: Evolution, development and functions. *J. Integr. Plant Biol.* **55**, 294–388 (2013). [doi:10.1111/jipb.12041](https://doi.org/10.1111/jipb.12041) [Medline](#)
11. R. Hedrich, V. Salvador-Recatalà, I. Dreyer, Electrical wiring and long-distance plant communication. *Trends Plant Sci.* **21**, 376–387 (2016). [doi:10.1016/j.tplants.2016.01.016](https://doi.org/10.1016/j.tplants.2016.01.016) [Medline](#)
12. J. Tilsner, W. Nicolas, A. Rosado, E. M. Bayer, Staying Tight: Plasmodesmal membrane contact sites and the control of cell-to-cell connectivity in plants. *Annu. Rev. Plant Biol.* **67**, 337–364 (2016). [doi:10.1146/annurev-arplant-043015-111840](https://doi.org/10.1146/annurev-arplant-043015-111840) [Medline](#)
13. J. Y. Lee, X. Wang, W. Cui, R. Sager, S. Modla, K. Czymmek, B. Zybaliiov, K. van Wijk, C. Zhang, H. Lu, V. Lakshmanan, A plasmodesmata-localized protein mediates

- crosstalk between cell-to-cell communication and innate immunity in Arabidopsis. *Plant Cell* **23**, 3353–3373 (2011). [doi:10.1105/tpc.111.087742](https://doi.org/10.1105/tpc.111.087742) [Medline](#)
14. A. Levy, M. Erlanger, M. Rosenthal, B. L. Epel, A plasmodesmata-associated beta-1,3-glucanase in Arabidopsis. *Plant J.* **49**, 669–682 (2007). [doi:10.1111/j.1365-313X.2006.02986.x](https://doi.org/10.1111/j.1365-313X.2006.02986.x) [Medline](#)
  15. E. D. Vincill, A. E. Clarin, J. N. Molenda, E. P. Spalding, Interacting glutamate receptor-like proteins in Phloem regulate lateral root initiation in Arabidopsis. *Plant Cell* **25**, 1304–1313 (2013). [doi:10.1105/tpc.113.110668](https://doi.org/10.1105/tpc.113.110668) [Medline](#)
  16. A. C. Furch, A. J. E. van Bel, M. D. Fricker, H. H. Felle, M. Fuchs, J. B. Hafke, Sieve element Ca<sup>2+</sup> channels as relay stations between remote stimuli and sieve tube occlusion in *Vicia faba*. *Plant Cell* **21**, 2118–2132 (2009). [doi:10.1105/tpc.108.063107](https://doi.org/10.1105/tpc.108.063107) [Medline](#)
  17. E. E. Farmer, D. Gasperini, I. F. Acosta, The squeeze cell hypothesis for the activation of jasmonate synthesis in response to wounding. *New Phytol.* **204**, 282–288 (2014). [doi:10.1111/nph.12897](https://doi.org/10.1111/nph.12897) [Medline](#)
  18. J. S. Marvin, B. G. Borghuis, L. Tian, J. Cichon, M. T. Harnett, J. Akerboom, A. Gordus, S. L. Renninger, T.-W. Chen, C. I. Bargmann, M. B. Orger, E. R. Schreiter, J. B. Demb, W.-B. Gan, S. A. Hires, L. L. Looger, An optimized fluorescent probe for visualizing glutamate neurotransmission. *Nat. Methods* **10**, 162–170 (2013). [doi:10.1038/nmeth.2333](https://doi.org/10.1038/nmeth.2333) [Medline](#)
  19. G. Lohaus, H. W. Heldt, Assimilation of gaseous ammonia and the transport of its products in barley and spinach leaves. *J. Exp. Bot.* **48**, 1779–1786 (1997).
  20. E. Hunt, S. Gattolin, H. J. Newbury, J. S. Bale, H.-M. Tseng, D. A. Barrett, J. Pritchard, A mutation in amino acid permease AAP6 reduces the amino acid content of the Arabidopsis sieve elements but leaves aphid herbivores unaffected. *J. Exp. Bot.* **61**, 55–64 (2010). [doi:10.1093/jxb/erp274](https://doi.org/10.1093/jxb/erp274) [Medline](#)
  21. J. Sandström, J. Pettersson, Amino-acid-composition of phloem sap and the relation to intraspecific variation in pea aphid (*Acyrtosiphon-Pisum*) performance. *J. Insect Physiol.* **40**, 947–955 (1994). [doi:10.1016/0022-1910\(94\)90133-3](https://doi.org/10.1016/0022-1910(94)90133-3)
  22. H. W. Choi, D. F. Klessig, DAMPs, MAMPs, and NAMPs in plant innate immunity. *BMC Plant Biol.* **16**, 232 (2016). [doi:10.1186/s12870-016-0921-2](https://doi.org/10.1186/s12870-016-0921-2) [Medline](#)
  23. M. Toyota, S. Gilroy, Gravitropism and mechanical signaling in plants. *Am. J. Bot.* **100**, 111–125 (2013). [doi:10.3732/ajb.1200408](https://doi.org/10.3732/ajb.1200408) [Medline](#)
  24. S. J. Clough, A. F. Bent, Floral dip: A simplified method for *Agrobacterium*-mediated transformation of *Arabidopsis thaliana*. *Plant J.* **16**, 735–743 (1998). [doi:10.1046/j.1365-313x.1998.00343.x](https://doi.org/10.1046/j.1365-313x.1998.00343.x) [Medline](#)
  25. A. Lenglet, D. Jašlan, M. Toyota, M. Mueller, T. Müller, G. Schönknecht, I. Marten, S. Gilroy, R. Hedrich, E. E. Farmer, Control of basal jasmonate signalling and defence through modulation of intracellular cation flux capacity. *New Phytol.* **216**, 1161–1169 (2017). [doi:10.1111/nph.14754](https://doi.org/10.1111/nph.14754) [Medline](#)
  26. N. F. Keinath, R. Waadt, R. Brugman, J. I. Schroeder, G. Grossmann, K. Schumacher, M. Krebs, Live Cell Imaging with R-GECO1 Sheds Light on flg22- and Chitin-Induced Transient [Ca<sup>2+</sup>]<sub>cyt</sub> Patterns in Arabidopsis. *Mol. Plant* **8**, 1188–1200 (2015). [doi:10.1016/j.molp.2015.05.006](https://doi.org/10.1016/j.molp.2015.05.006) [Medline](#)

27. T. R. Vincent, M. Avramova, J. Canham, P. Higgins, N. Bilkey, S. T. Mugford, M. Pitino, M. Toyota, S. Gilroy, A. J. Miller, S. A. Hogenhout, D. Sanders, Interplay of plasma membrane and vacuolar ion channels, together with BAK1, elicits rapid cytosolic calcium elevations in Arabidopsis during aphid feeding. *Plant Cell* **29**, 1460–1479 (2017). [Medline](#)
28. W. G. Choi, D. M. Roberts, Arabidopsis NIP2;1, a major intrinsic protein transporter of lactic acid induced by anoxic stress. *J. Biol. Chem.* **282**, 24209–24218 (2007). [doi:10.1074/jbc.M700982200](https://doi.org/10.1074/jbc.M700982200) [Medline](#)
29. S. A. Bustin, V. Benes, J. A. Garson, J. Hellemans, J. Huggett, M. Kubista, R. Mueller, T. Nolan, M. W. Pfaffl, G. L. Shipley, J. Vandesompele, C. T. Wittwer, The MIQE guidelines: Minimum information for publication of quantitative real-time PCR experiments. *Clin. Chem.* **55**, 611–622 (2009). [doi:10.1373/clinchem.2008.112797](https://doi.org/10.1373/clinchem.2008.112797) [Medline](#)
30. A. N. Poudel, T. Zhang, M. Kwasniewski, R. Nakabayashi, K. Saito, A. J. Koo, Mutations in jasmonoyl-L-isoleucine-12-hydroxylases suppress multiple JA-dependent wound responses in Arabidopsis thaliana. *Biochim. Biophys. Acta* **1861** (9 Pt B), 1396–1408 (2016). [doi:10.1016/j.bbailip.2016.03.006](https://doi.org/10.1016/j.bbailip.2016.03.006) [Medline](#)
31. W. G. Choi, M. Toyota, S. H. Kim, R. Hilleary, S. Gilroy, Salt stress-induced Ca<sup>2+</sup> waves are associated with rapid, long-distance root-to-shoot signaling in plants. *Proc. Natl. Acad. Sci. U.S.A.* **111**, 6497–6502 (2014). [doi:10.1073/pnas.1319955111](https://doi.org/10.1073/pnas.1319955111) [Medline](#)
32. W. G. Choi, S. J. Swanson, S. Gilroy, High-resolution imaging of Ca<sup>2+</sup>, redox status, ROS and pH using GFP biosensors. *Plant J.* **70**, 118–128 (2012). [doi:10.1111/j.1365-3113X.2012.04917.x](https://doi.org/10.1111/j.1365-3113X.2012.04917.x) [Medline](#)
33. T. Nagai, S. Yamada, T. Tominaga, M. Ichikawa, A. Miyawaki, Expanded dynamic range of fluorescent indicators for Ca<sup>2+</sup> by circularly permuted yellow fluorescent proteins. *Proc. Natl. Acad. Sci. U.S.A.* **101**, 10554–10559 (2004). [doi:10.1073/pnas.0400417101](https://doi.org/10.1073/pnas.0400417101) [Medline](#)
34. N. C. Dengler, The shoot apical meristem and development of vascular architecture. *Can. J. Bot.* **84**, 1660–1671 (2006). [doi:10.1139/b06-126](https://doi.org/10.1139/b06-126)
35. J. M. Davis, M. P. Gordon, B. A. Smit, Assimilate movement dictates remote sites of wound-induced gene expression in poplar leaves. *Proc. Natl. Acad. Sci. U.S.A.* **88**, 2393–2396 (1991). [doi:10.1073/pnas.88.6.2393](https://doi.org/10.1073/pnas.88.6.2393) [Medline](#)